Environ Earth Sci (2017) 76:265
DOI 10.1007/s12665-017-6590-0

ORIGINAL ARTICLE

Trace elements, REEs and stable isotopes (B, Sr) in GAS groundwater, São Paulo State, Brazil

Daniel Marcos Bonotto[1] · **Trevor Elliot**[2]

Received: 16 January 2017 / Accepted: 24 March 2017 / Published online: 30 March 2017

Abstract This investigation was carried out in the Guarani Aquifer System (GAS) following a transect in São Paulo State, Brazil, and involved the analysis of trace elements, REEs and stable isotopes (B, Sr) in both rainwater and groundwater samples (the latter sampled from tube wells drilled in 10 cities). The Brazilian Code for Mineral Waters (BCMW) has been adopted for classifying the groundwaters according to their temperature and was useful for identifying the major trends of the hydrochemical data. Three water categories are identified: (<25 °C), hypothermal (values ranging from 25 to 33 °C) and hyperthermal (>38 °C). The hyperthermal waters exhibited geostatic pressures >250 bar, whereas the cold/hypothermal waters values <100 bar. REEs concentrations were higher at the monitoring point BCS (Bernardino de Campos). Dissolved strontium in the groundwater behaves like other alkaline earth metals (calcium and barium) in samples collected along the studied transect. The hyperthermal waters tended to exhibit similar $^{87}Sr/^{86}Sr$ ratios (between 0.7088 and 0.7099), approximately corresponding to the value of ca. 0.709 for seawater Sr isotopic ratio at the end of the Proterozoic. The cold and hypothermal waters exhibited lower B contents than the hyperthermal waters. The $\delta^{11}B$ ranged from −8.1 to +12.0‰, where the $\delta^{11}B$-values in cold/hypothermal waters were characteristically positive in clear distinction to the negative $\delta^{11}B$ signatures found in hyperthermal waters.

Keywords Stable isotopes · Rare earth elements · Groundwater · Guarani Aquifer System · Paraná sedimentary basin

Introduction

The huge, transboundary Guarani Aquifer System (GAS) in South America has been investigated using many different approaches since the 1970s, many of the studies arising out of the IAEA-sponsored Global Environment Fund (GEF)—Guarani Aquifer Program for Groundwater Resource Sustainability and Environmental Protection (Foster et al. 2006). The GAS represents an important hydrological resource for about 90 million inhabitants living in the Mercosur nations, and its waters are used extensively for potable supply with many water supply systems using its waters at least as part of their networks.

As a consequence, several water resource investigations have been undertaken detailing hydrochemistry, stable isotopes (H, O, C, S) and radionuclides (^{14}C, ^{36}Cl, ^{238}U, ^{234}U, ^{226}Ra, ^{222}Rn, ^{228}Ra, ^{210}Pb, ^{210}Po) to investigate groundwater flow patterns and ages, paleoclimatic conditions, mineral dissolution and precipitation processes, water qualities and resource availability (e.g., Sracek and Hirata 2002; Bonotto and Caprioglio 2002; Bonotto 2004, 2006, 2011, 2012, 2013; Bonotto and Mello 2006; Bonotto and Bueno 2008; Bonotto and Armada 2008; Cresswell and Bonotto 2008; Bonotto et al. 2009a, b; Gastmans et al. 2010a, b; Hirata et al. 2011; i Gil and Bonotto 2015).

Multiple studies have been realized already in the Paraná sedimentary basin focusing on the rare earth

✉ Daniel Marcos Bonotto
danielbonotto@yahoo.com.br

[1] Instituto de Geociências e Ciências Exatas-IGCE, Universidade Estadual Paulista-UNESP, Av. 24-A No. 1515, P.O. Box 178, Rio Claro, São Paulo CEP 13506-900, Brazil

[2] School of Natural and Built Environment (SNBE), Queeńs University Belfast, Stranmillis Road, Belfast BT9 5AG, Northern Ireland, UK

elements (REEs) distributions in the igneous basaltic rocks (e.g., Marques et al. 1999). However, there is a lack of investigation focusing on their presence in groundwater, mainly due to the difficulties for their quantification in the liquid phase as a consequence of the very low dissolved contents. Unlike major ions chemistry, the REEs abundance exhibits patterns reflecting those of the host aquifers, thus constituting useful tracers of groundwater flow in aquifers where the mineralogy may vary (cf. Tweed et al. 2006).

This paper focuses a single transect previously studied in São Paulo State, Brazil, also including additional monitoring points sampled there. The REEs abundance has been determined in rainwater and groundwater samples, as well as other dissolved trace elements not previously discussed for the GAS and also the stable isotopes of strontium ($^{87}Sr/^{86}Sr$ ratios) and boron ($\delta^{11}B$-values) in some selected wells. Such novel database has allowed to perform new insights on the water/rock–soil interactions taking place in this GAS portion at São Paulo State, with possible implications to other areas of its occurrence in the Paraná sedimentary basin.

Study area and experimental

The GAS consists of Triassic–Jurassic age aeolian–fluvio–lacustrine sandstones confined by thick Cretaceous basalt flows of the Serra Geral Formation and extends over some 1.2 million km^2 within the Paraná sedimentary basin comprising southern Brazil, eastern Paraguay, NW Uruguay and the NE extreme corner of Argentina. Table 1 shows that the basalts and diabases package of the Serra Geral Formation overlying the GAS occur in all wells sampled in this study, except in São Pedro (SPO) city. The lithological description of the bores (Table 1) indicates that the main GAS sediments (Botucatu Formation and Pirambóia Formation) in the study area overlie greatly variable thick layers of the Passa Dois Group, Tubarão Group and Paraná Group sediments at Paraguaçu Paulista (PPA), Presidente Prudente (PPE) and Presidente Epitácio (PEO) municipalities.

Rainwater sample was collected at a station located in the GAS recharge beds close to Rio Claro city area (Fig. 1) and sampled during the middle of the wet season

Table 1 Location and description of the tubular wells drilled at the GAS—Guarani Aquifer System, at São Paulo State, Brazil, whose waters were analyzed in this paper

Sample code	Site	State	Latitude	Longitude	Altitude (m)	Depth (m)	GP (bar)	Stratigraphy
ITI	Itirapina	SP	22°15′13″S	47°49′05″W	880	129	0.9	BP (0–69); DI (69–115); BP (115–129)
SPO	São Pedro	SP	22°32′07″S	47°54′33″W	590	150	0.9	BP (0–150)
AVR	Avaré	SP	23°06′46″S	48°54′33″W	640	150	10.2	M (0–8); BA (8–12); SG (12–35); BP (35–150)
SUT	Sarutaiá	SP	23°16′03″S	49°29′05″W	750	152	7.8	M (0–4); SG (4–26); BO (26–145); DI (145–152)
ASB	Águas de Santa Bárbara	SP	22°52′24″S	49°13′38″W	560	120	3.0	SG (0–8); BO (8–56); SG (56–104); BO (104–120)
BCS	Bernardino de Campos	SP	23°01′41″S	49°29′05″W	660	509	87.4	M (0–21); SG (21–327); BO (327–402); PI (402–509)
SCP	Santa Cruz do Rio Pardo	SP	22°54′56″S	49°39′05″W	440	124	31.1	SG (0–114); BO (114–124)
PPA	Paraguaçu Paulista	SP	22°25′21″S	50°33′38″W	474	3663	258.7	BA (0–64); SG(64–974); BO (974–1250); PD (1250–2050); TU (2050–3554); PA (3554–3663)
PPE	Presidente Prudente	SP	22°06′45″S	51°22′43″W	407	1800	382.0	BA (0–218); SG (218–1440); BO (1440–1570); PI (1570–1730); PD (1730–1800)
PEO	Presidente Epitácio	SP	21°46′29″S	52°05′27″W	258	3953	430.4	BA (0–90); SG (90–1623); BO (1623–1976); PI–PD–TU–PA (?–?)
RCL	Rio Claro	SP	22°24′41″S	47°33′41″W	625	–	–	–

RCL, rainwater; GP, geostatic pressure (Castany 1982), M, weathered mantle; DI, diabase sill; BA, Bauru Group (sandstones, siltstones, mudstones, carbonatic nodules); SG, Serra Geral Formation (basalts, diabases); BO, Botucatu Formation (eolic sandstones); PI, Pirambóia Formation (fluvial sandstones); BP, Undifferentiated Botucatu–Pirambóia Formations; PD, Passa Dois Group (siltstones, mudstones, shales, limestones); TU, Tubarão Group (sandstones, conglomerates, diamictites, tillites, siltstones, shales, rhythmites, silex); PA, Paraná Group (Devonian) (sandstones, conglomerates)

In parentheses = depth range (in meters). Major lithologies according to Almeida and Melo (1981)

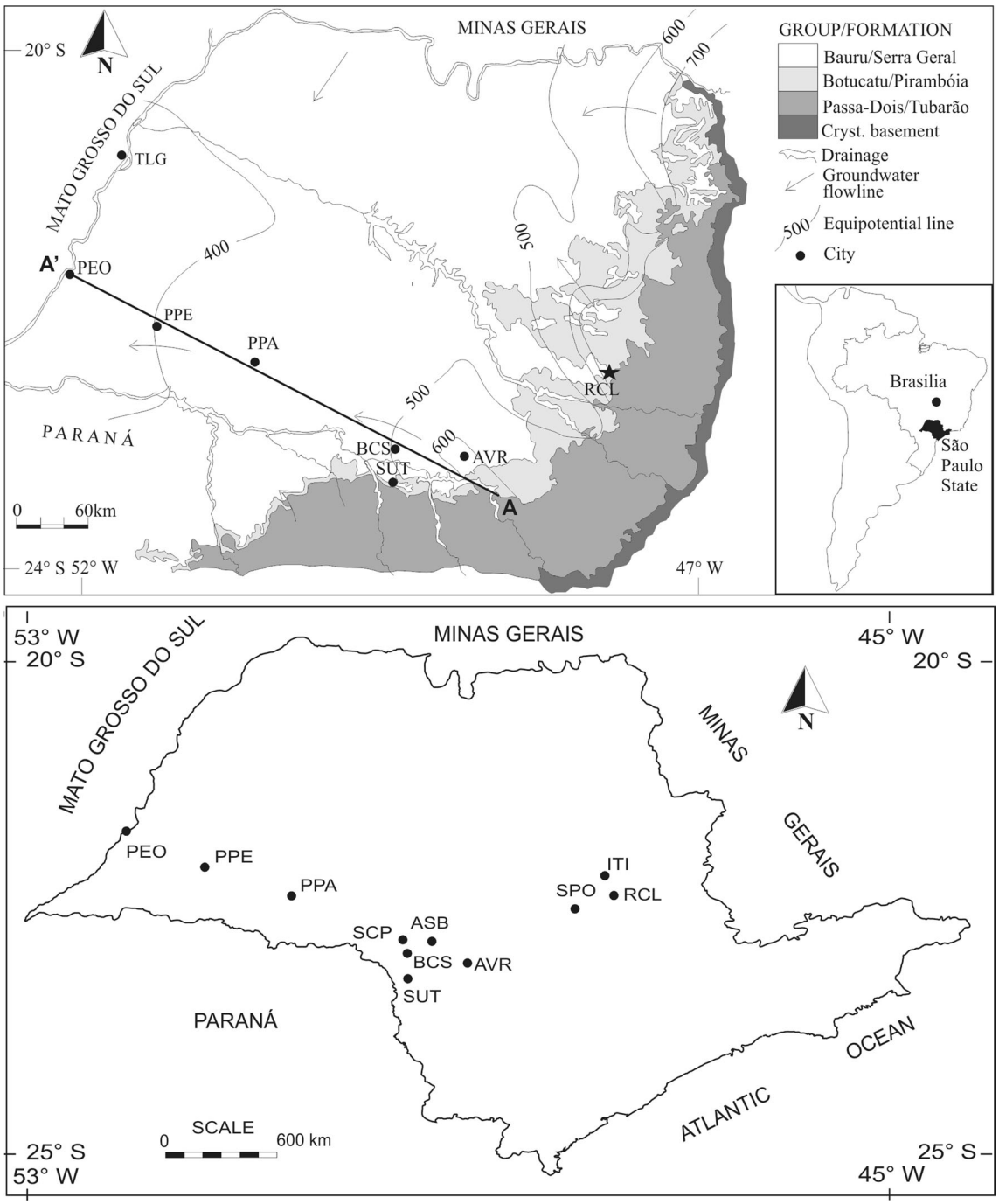

Fig. 1 (*top*) Simplified map modified from Silva (1983) showing the outcrop and groundwater flow direction in the GAS, São Paulo State, Brazil, as well the transect AA' from Avaré up to Presidente Epitácio (SE–NW direction); the star symbol indicates the location of the rainwater monitoring point (RCL). (*bottom*) Location at São Paulo State of all sampling sites, whose codes are: AVR, Avaré; SUT, Sarutaiá; ASB, Águas de Santa Bárbara; BCS, Bernardino de Campos; PPA, Paraguaçu Paulista; PPE, Presidente Prudente; PEO, Presidente Epitácio; SCP, Santa Cruz do Rio Pardo; SPO, São Pedro; ITI, Itirapina; RCL, Rio Claro

(December 2009) to ensure collection of pristine (less affected by evaporation) signature. Samples were collected with bulk (dry and wet deposition) collectors consisting of large rectangular funnels coupled to polyethylene flasks (25 L) that allowed rapidly sample the same rainfall event, without the need of specific protocol for collections performed over long periods of time (Pelicho et al. 2006).

Groundwater samples in this study provided from 10 municipalities in São Paulo State (Fig. 1, bottom). They were collected along the transect AA′ in São Paulo State

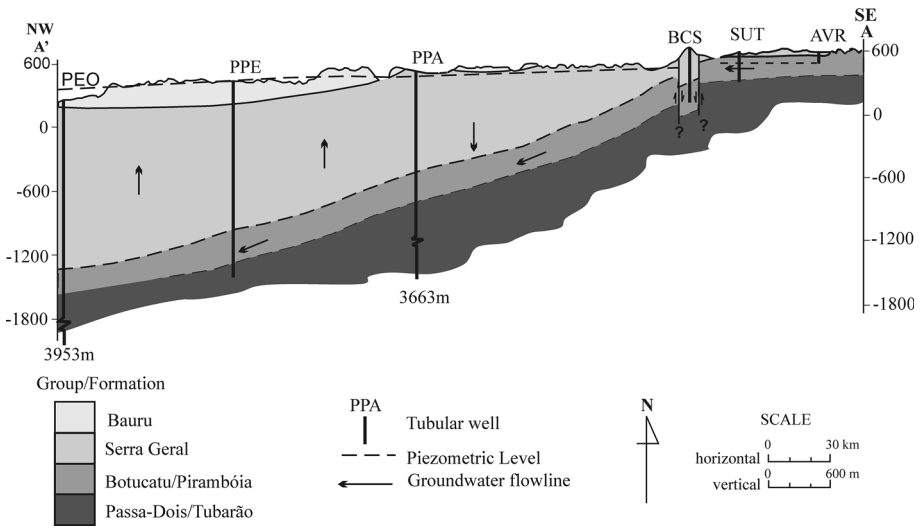

Fig. 2 Simplified geological cross section along transect AA' according to Silva (1983) showing the depth and stratigraphy of the bores, as well the groundwater flow direction in the GAS. The main lithologies are (Almeida and Melo 1981): Bauru, sandstones, siltstones, mudstones, carbonatic nodules; Serra Geral, basalts, diabases; Botucatu/Pirambóia, sandstones; Passa Dois/Tubarão, sandstones, conglomerates, siltstones, mudstones, shales, limestones, diamictites, tillites, rhythmites

already focused in previous hydrogeochemical investigations (Fig. 1, top): AVR—Avaré, SUT—Sarutaiá, BCS—Bernardino de Campos, PPA—Paraguaçu Paulista, PPE—Presidente Prudente and PEO—Presidente Epitácio (Sracek and Hirata 2002; Bonotto 2006; Cresswel and Bonotto 2008; i Gil and Bonotto 2015). Four additional samples were collected at São Paulo State from 120- to 150-m-deep tube wells drilled into the GAS recharge beds at Itirapina (ITI), São Pedro (SPO), Águas de Santa Bárbara (ASB) and Santa Cruz do Rio Pardo (SCP) municipalities (Fig. 1, bottom).

Both rainwater and groundwater samples were stored in polyethylene bottles, with the field temperature, dissolved oxygen, pH, redox potential (Eh), electrical conductivity (EC) and alkalinity readings being performed according to the protocols described by Bonotto (2006). The filled bottles were transported up to LABIDRO-Isotopes and Hydrochemistry Laboratory of UNESP at Rio Claro city, where aliquots were divided for evaluating the major/trace elements, REEs and stable (Sr and B) isotopes. Suspended solids were separated on filtering the samples through a 47-mm-diameter Millipore membrane of 0.45-μm porosity. The dry residue (DR) (which equates to ~TDS, total dissolved solids) content and free dissolved CO_2 data have been given in Bonotto (2006).

The filtered aliquots for dissolved cations were preserved with HNO_3 or HCl. Na and K were measured by atomic absorption spectrometry (AAS); Ca, Mg and Si contents by inductively coupled plasma atomic emission spectrometry (ICP-AES). Major anions measurements on unacidified aliquots for chloride, fluoride, nitrate and sulfate were taken using potentiometry and colorimetry as reported by Bonotto (2006).

Trace elements Al, B, Br, Li, Ba, Mo, Cr, Zn, As, Rb and Sr were all quantified by inductively coupled plasma mass spectrometry (ICP-MS) analysis performed at Nicholas School of the Environment, Duke University, USA.

The aliquots (10–50 L) for REEs analysis were acidified to pH < 2 on using HCl, and about 1 g $FeCl_3$ added. The REEs were co-precipitated on $Fe(OH)_3$ by increasing the pH to 7–8 through addition of concentrated NH_4OH solution. The precipitate was recovered, dissolved in 8 M HCl, and Fe^{3+} was extracted into an equal volume of isopropyl ether. The acid solution containing REEs then was evaporated to dryness, and the dry residue dissolved with 1.75 M HCl to a volume of 20 mL. The acidic REEs-bearing solution was purified by cation-exchange chromatography on a Cl^- column of 100–200 mesh Dowex resin. The REEs then were eluted from the Cl^- column with 4 M HCl and after evaporation to dryness was dissolved in 20 mL of 1.75 M HCl. The REEs concentration in the acid solution then was measured by ICP-AES Model 3410 Spectrometer, Fisons Instruments at LABOGEO—Geochemistry Laboratory, UNESP, Rio Claro city. The detection limit (DL) for the lanthanides was: La = 9.18 μg/L; Ce = 21.87 μg/L; Nd = 8.95 μg/L; Sm = 4.14 μg/L; Eu = 1.09 μg/L; Gd = 15.77 μg/L; Dy = 8.74 μg/L; Er = 0.66 μg/L; Yb = 0.79 μg/L; Lu = 0.56 μg/L.

Analyses of strontium and boron isotopes in groundwater along transect AA′ (Fig. 2) were made at Nicholas School of the Environment, Duke University, USA, using a fully automated Thermo Scientific Triton Thermal Ionization Mass Spectrometer (TIMS) with Virtual Amplifiers, Dynamic Zoom and all-carbon plug-in Faraday cups, whose abundance sensitivity is ~1 ppm. The technique included the use of a low-blank matrix solution that enhances BO_2^- ionization and provides a stable ion beam with minimum isotopic fractionation for boron isotopes (Vengosh et al. 1989); the boron blank levels tested by isotope dilution methodology were less than 15 pg. The Sr isotopes data were expressed as $^{87}Sr/^{86}Sr$ ratios, whereas

Table 2 Results of the analysis of the rainwater and groundwater samples considered in this paper

Parameter	Unit	ITI	SPO	AVR	SUT	ASB	BCS	SCP	PPA	PPE	PEO	RCL
Temp.	°C	25	32	23	23	28	28	24	43	63	70	25
pH	–	4.03	5.89	5.94	6.39	7.58	6.60	8.26	9.64	8.80	8.70	5.90
Eh	mV	208	196	144	164	112	200	457	−66	−55	−72	–
Diss. O_2	mg/L	8.0	9.5	6.0	8.0	8.5	7.0	9.0	3.2	2.4	2.8	–
Diss. CO_2	mg/L	300	16	180	30	3	45	0.3	0.1	0.5	0.6	–
EC	µS/cm	70	13	70	70	160	160	110	520	910	760	110
DR[1]	mg/L	200	100	300	200	200	300	150	400	200	600	–
Si	mg/L	3.7	4.5	24.4	20.8	18.3	18.1	11.2	21.4	13.3	16.8	–
HCO_3^- + CO_3^{2-}	mg/L	2	6	70	41	73	102	36	72	216	222	7
Cl^-	mg/L	<0.15	<0.15	<0.15	<0.15	<0.15	<0.15	6.6	9.6	110.0	56.0	1.1
NO_3^-	mg/L	0.7	1.2	0.5	0.6	0.6	0.7	0.6	0.7	0.7	0.6	3.5
SO_4^{2-}	mg/L	<0.3	<0.3	<0.3	<0.3	0.5	0.5	<0.3	9.3	69.8	81.7	1.2
F^-	mg/L	<0.02	<0.02	<0.02	0.05	<0.02	<0.02	0.84	1.60	8.80	6.60	–
Br^-	mg/L	–	–	0.02	0.01	–	0.01	–	0.04	0.17	0.06	0.01
Na	mg/L	0.5	0.8	3.3	4.9	7.3	14.5	22.6	117.0	214.0	178.0	0.9
K	mg/L	0.18	0.69	1.55	2.73	3.07	1.09	0.56	0.55	2.12	1.39	0.30
Ca	mg/L	0.21	0.21	8.58	7.75	25.50	20.10	4.43	0.52	4.83	1.99	0.83
Mg	mg/L	0.18	0.41	4.18	1.21	0.90	2.14	<0.10	<0.10	0.71	<0.10	0.25
Li	µg/L	–	–	0.9	2.0	–	3.0	–	19.8	57.4	29.5	0.1
Al	µg/L	–	–	3.4	3.0	–	5.9	–	78.1	58.4	71.7	17.8
B	µg/L	–	–	0.8	4.0	–	4.6	8	318.6	2063.0	897.8	5.0
Rb	µg/L	–	–	3.1	5.0	–	1.0	–	0.8	5.3	1.3	1.2
Sr	µg/L	–	–	98.7	83.1	–	146.8	–	5.5	144.0	69.1	4.1
Ba	µg/L	13.0	35.0	16.6	11.5	9.0	10.9	1.0	0.2	29.3	12.9	3.1
Zn	µg/L	30.0	14.0	2.2	6.6	10.0	0.6	7.0	22.8	18.0	4.9	0.1
Cr	µg/L	–	–	0.98	1.39	–	2.05	–	3.53	15.58	2.27	0.40
As	µg/L	–	–	0.03	0.44	–	0.10	–	19.62	4.73	6.95	0.24
Mo	µg/L	–	–	<0.01	<0.01	–	0.02	–	0.65	4.60	3.59	0.90
U[a]	µg/L	0.01	0.09	0.09	0.10	4.82	0.71	0.11	0.31	0.06	1.01	–
$^{234}U/^{238}U$[a]	A.R.	1.81	1.29	6.32	3.87	2.19	5.31	2.24	1.77	1.61	4.29	–
^{222}Rn[b]	Bq/L	38.4	57.2	40.8	4.1	12.5	86.5	45.9	44.5	2.5	37.3	–
^{226}Ra[b]	Bq/L	0.12	0.14	0.40	0.31	0.18	0.42	0.32	0.44	0.19	0.24	–
$\delta^{11}B$	‰	–	–	–	+12.0	–	+10.9	–	−6.6	−7.3	−8.1	–
$^{87}Sr/^{86}Sr$	–	–	–	–	0.7072	0.7117	–	0.7130	–	0.7094	0.7099	0.7088	–

DR, dry residue

[a] Data reported by Bonotto (2006); [b]Data reported by Bonotto (2004)

the B isotopes as $\delta^{11}B$ (in ‰), which was determined by the equation:

$$\delta^{11}B = \{[(^{11}B/^{10}B)_{sample}/(^{11}B/^{10}B)_{std}] - 1\} \times 1000 \quad (1)$$

where $(^{11}B/^{10}B)_{std}$ is the $^{11}B/^{10}B = 4.04367$ of boric acid (SRM 951).

Results

All hydrochemical data for the rainwater and groundwater samples are reported in Tables 2 and 3.

Discussion

Water quality, hydrochemical trends and temperature

WHO (2011) has established guideline values for the following parameters in Table 2 that are of health significance in drinking water: nitrate (50 mg/L), fluoride (1.5 mg/L), boron (2400 µg/L), barium (700 µg/L), chromium (50 µg/L), arsenic (10 µg/L), uranium (30 µg/L) and ^{226}Ra (1 Bq/L). Concentrations exceed the maximum admissible concentration for fluoride in the hyperthermal

Table 3 REE concentration of groundwater and rainwater samples analyzed in this paper

Sample code[a]	Unit	Volume (L)	La	Ce	Nd	Sm	Eu	Gd	Dy	Er	Yb	Lu
ITI	ng/L	43.5	45.1	36.6	8.1	3.7	9.9	45.1	7.2	7.2	7.2	1.4
ITI	ng/L	43.2	47.0	43.7	9.3	4.9	11.0	47.0	7.5	6.2	6.2	1.1
SPO	ng/L	43.9	23.6	25.9	15.2	2.8	1.0	5.4	4.8	3.3	2.8	0.8
AVR	ng/L	43.9	38.4	44.5	28.8	5.3	1.8	5.9	4.4	2.6	2.3	0.5
SUT	ng/L	10.0	15.0	30.0	9.0	3.0	25.0	3.0	<DL	<DL	1.0	1.0
SUT	ng/L	45.1	17.4	22.1	10.1	1.1	<DL	3.6	<DL	2.1	2.0	0.7
ASB	ng/L	45.1	20.0	19.1	12.2	2.8	1.0	3.2	<DL	2.0	1.8	0.3
BCS	ng/L	45.7	281.2	494.4	276.3	45.7	19.0	42.6	28.6	13.0	7.1	1.0
SCP	ng/L	46.3	24.7	28.4	13.0	2.3	<DL	3.4	<DL	2.2	2.4	0.6
PPA	ng/L	10.0	<DL	<DL	<DL	1.0	2.0	<DL	<DL	<DL	1.0	<DL
PPE	ng/L	45.3	19.9	23.3	10.9	1.8	<DL	2.8	3.8	2.9	3.5	0.7
PEO	ng/L	44.1	16.0	17.5	7.0	0.6	<DL	<DL	<DL	<DL	1.5	0.3
RCL[b]	ng/L	50.0	29.2	29.1	12.8	2.2	<DL	2.7	<DL	<DL	0.4	0.2
NASC	µg/g	–	34.0	66.7	30.1	5.8	1.16	5.12	4.67	2.73	2.67	0.41
NASC-normalized REE abundance												
ITI	$\times 10^{-7}$		13.3	5.5	2.7	6.4	85.8	88.2	15.4	26.3	26.9	33.9
ITI	$\times 10^{-7}$		13.8	6.6	3.1	8.4	95.2	91.8	16.1	22.6	23.2	26.8
SPO	$\times 10^{-7}$		7.0	3.9	5.1	4.8	8.9	10.5	10.4	12.2	10.6	18.3
AVR	$\times 10^{-7}$		11.3	6.7	9.6	9.2	15.1	11.5	9.3	9.4	8.5	12.7
SUT	$\times 10^{-7}$		4.4	4.5	3.0	5.2	215.5	5.9	<DL	<DL	3.8	24.4
SUT	$\times 10^{-7}$		5.1	3.3	3.3	1.9	<DL	7.0	<DL	7.6	7.3	16.3
ASB	$\times 10^{-7}$		5.9	2.9	4.0	4.8	9.0	6.3	<DL	7.3	6.7	8.3
BCS	$\times 10^{-7}$		82.7	74.1	91.8	78.8	164.2	83.3	61.1	47.7	26.7	23.7
SCP	$\times 10^{-7}$		7.3	4.3	4.3	4.0	<DL	6.6	<DL	8.0	8.9	15.4
PPA	$\times 10^{-7}$		<DL	<DL	<DL	1.7	17.2	<DL	<DL	<DL	3.8	<DL
PPE	$\times 10^{-7}$		5.9	3.5	3.6	3.1	<DL	5.5	8.2	10.5	13.0	16.1
PEO	$\times 10^{-7}$		4.7	2.6	2.3	1.0	<DL	<DL	<DL	<DL	5.6	7.1
RCL[b]	$\times 10^{-7}$		8.6	4.4	4.3	3.8	<DL	5.2	<DL	<DL	1.6	5.1

NASC, North American Shale Composite (Goldstein and Jacobsen 1988); DL, detection limit

[a] Site location in Fig. 1; [b]Rainwater

(>38 °C) waters PPA, PPE and PEO, as well for arsenic in PPA. However, none of these waters is used for human consumption, only for recreational (thermal swimming pools) purposes.

For dissolved radionuclides, the adoption of a dose conversion factor (DCF: IAEA 1996; WHO 2011) is required to estimate effective doses from ingestion of radionuclides in waters. There is, however, no consensus in the literature on the DCF value for ^{222}Rn. A value of 10^{-8} Sv/Bq resulting from the application of a modified ICRP model for the ^{222}Rn ingestion in water sometimes has been adopted (Kendall et al. 1988; Oliveira et al. 2001; Bonotto 2004). Bonotto (2011) suggested a value of 1.4×10^{-6} mSv/Bq that is utilized in this paper. Assuming an annual dietary water consumption of 2 L (WHO 2011) and applying this DCF to the ^{222}Rn activity concentration data (Table 2), it is possible to estimate the dose range due to ingested ^{222}Rn as 0.002–0.09 mSv/year. Such annual doses are lower than the WHO (2011) guideline reference value of 0.1 mSv/year for the ingestion of all radionuclides dissolved in drinking water.

The parameters pH and Eh reflect, respectively, the proton (pH) and electron (pe) activities in the environment. In natural systems, reactions in which both protons and electrons are transferred are common, effecting pH and Eh according to the following general trends: lower Eh values tend to occur under higher pH conditions, and higher Eh values are contrarily obtained under lower pH conditions (Baas Becking et al. 1960). There is little significant correlation ($r = -0.46$; $n = 10$) between the pH and Eh data in the study groundwaters. The Eh–pH diagram (Fig. 3) shows that the circulation environment for the waters is variable: reducing transitional acidic (ITI, SPO, SUT, AVR, BCS), oxidizing basic (SCP), transitional basic (ASB) and reducing basic (PPA, PPE, PEO).

^{238}U and ^{234}U are considered useful isotopes for the hydrogeochemical prospection for concealed, subsurface U

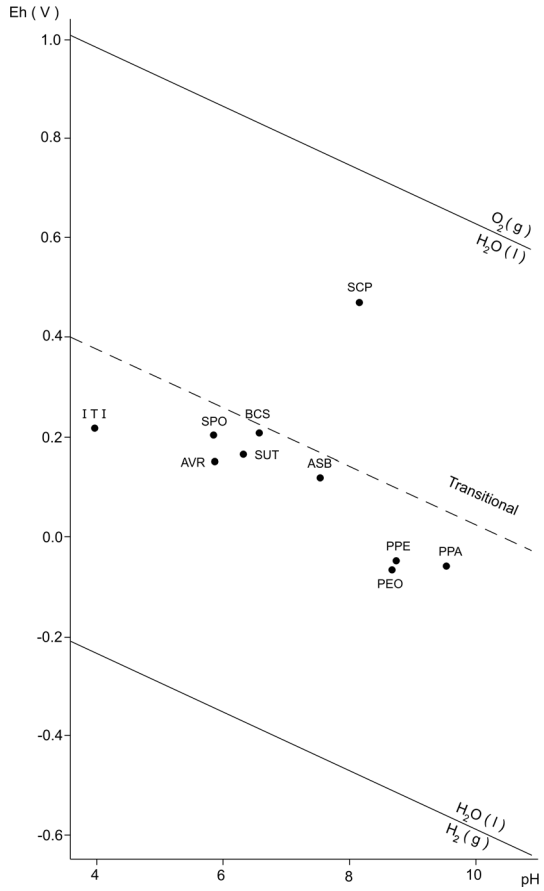

Fig. 3 Plotting of the pH and Eh data in the study area in an Eh–pH diagram (Krauskopf and Bird 1995). Codes: AVR, Avaré; SUT, Sarutaiá; ASB, Águas de Santa Bárbara; BCS, Bernardino de Campos; PPA, Paraguaçu Paulista; PPE, Presidente Prudente; PEO, Presidente Epitácio; SCP, Santa Cruz do Rio Pardo; SPO, São Pedro; ITI, Itirapina

deposits. The data for dissolved U content and $^{234}U/^{238}U$ activity ratio (AR) in the GAS groundwaters (Table 2) are plotted on a two-dimensional U content *vs.* AR diagram containing several areas of associative significance (Cowart and Osmond 1980; Osmond and Cowart 1981; Chatam et al. 1981). Most of the samples are categorized as reducing as defined also by the Eh–pH diagram. The groundwater sample SCP is oxidizing (Fig. 3) rather than reducing (U content vs. AR diagram; Bonotto 2006), perhaps due to a mixed signature or dominance of another couple).

The data for pH, EC, major cations (Na^+, K^+, Ca^{2+}, Mg^{2+}) and major anions ($HCO_3^- + CO_3^{2-}$, Cl^-, NO_3^-, SO_4^{2-}) in each groundwater sample have been autocorrelated with those of the rainwater. The following Pearson correlation coefficient values were found: ITI: $r = 0.99$; SPO: $r = 0.88$; AVR: $r = 0.70$; SUT: $r = 0.88$; ASB: $r = 0.92$; BCS: $r = 0.85$; SCP: $r = 0.95$; PPA: $r = 0.97$; PPE: $r = 0.96$; PEO: $r = 0.95$. These coefficients suggest a strong influence of the rainwater signature on the groundwater chemistry. Such behavior should be expected in the boreholes drilled close to the recharge beds (ITI, SPO, AVR, SUT, ASB, BCS and SCP) but not necessarily in the deeper (PPA, PPE and PEO) tube wells where higher water–rock interaction impacts might be expected. Thus, such major element criteria then are not particularly useful for discriminating unconfined and confined groundwater in the GAS.

Discrimination appears when the trace constituents (Br^-, Li, Al, B, Rb, Sr, Ba, Zn, Cr, As, Mo) and REEs in groundwater and rainwater are considered. The autocorrelations here are not significant for the boreholes close to the recharge beds (AVR: $r = 0.17$; SUT: $r = 0.17$; BCS: $r = 0.18$) nor particularly for those exploiting the deeper wells (PPA: $r = 0.36$; PPE: $r = 0.22$; PEO: $r = 0.26$). The lack of autocorrelation with rainwater emphasizes the sensitivity of minor/trace elements to discriminate groundwater processes (water–rock interactions) here; however, unlike for the case that strong autocorrelation with rainwater signatures implies lack of discrimination between unconfined/confined groundwater we cannot simply preclude the same here (as the deeper wells show a higher r than the recharge bed waters).

Temperature categories from the Brazilian Code for Mineral Waters (BCMW; DFPM 1966) also prove useful for discriminating the groundwater samples in this study (Table 2): cold (<25 °C: AVR, SUT, SCP); hypothermal (25–33 °C: ITI, SPO, ASB, BCS); and hyperthermal (>38 °C: PPA, PPE, PEO). Two major water groupings are identified: cold/hypothermal waters (Group I) and hyperthermal waters (Group II). Figure 4 shows that the Group I waters exhibit geostatic pressure <100 bar, dissolved O_2 >6 mg/L, positive Eh values, EC <160 µS/cm, sodium <23 mg/L, chloride <7 mg/L and sulfate <0.5 mg/L. The trace constituents Al, Li, F, Br, As and Mo then are seen to be enhanced in the Group II waters relative to the Group I waters (Fig. 5). Nevertheless, despite its usefulness, this temperature criterion when looking at only the major hydrochemical facies fails to show coherent discrimination of waters; for instance, the hyperthermal waters PPA, PPE and PEO are dominated by sodium and (bi)carbonate, the same occurring with the cold groundwater SCP.

REEs dissolved in groundwater and rainwater

REEs generally are lithophile in character and strongly enriched in the continental crust relative to mantle and oceanic crust. Their crustal enrichment factors decrease with increasing atomic number (Faure 1991) from 26.8 for La ($Z = 57$) to 4.9 for Lu ($Z = 71$). Systematic variation of the abundances of the REEs in the continental crust correlates with the decrease in their ionic radii (the so-called lanthanide contraction), which results from the progressive filling of 4f orbitals and the consequent contraction of their electron clouds (Faure 1991). Thus, effective ionic radii of the REEs decrease from 1.13 Å for La^{3+} to 0.94 Å for

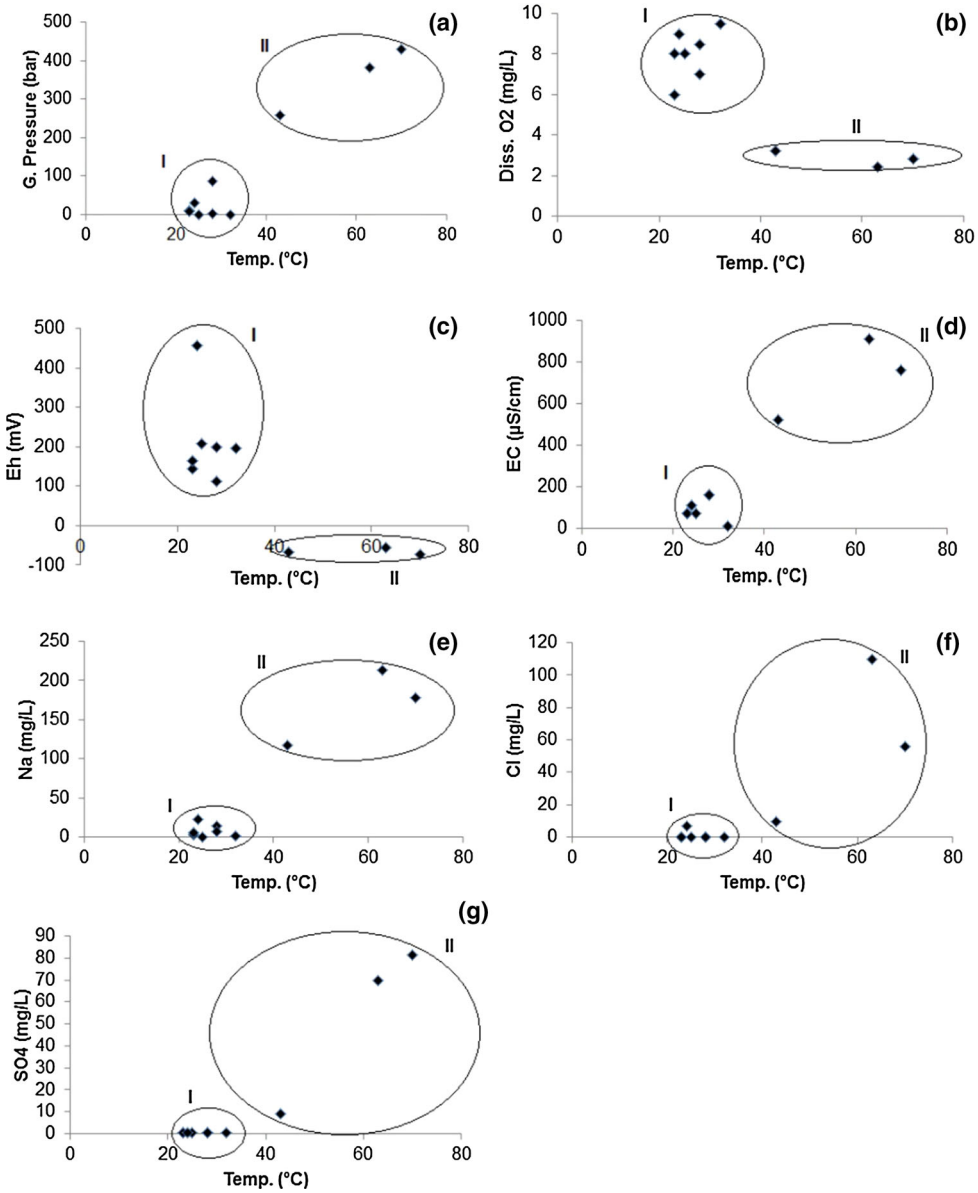

Fig. 4 **a** Geostatic pressure, **b** dissolved oxygen, **c** redox potential Eh, **d** electrical conductivity (EC), **e** sodium, **f** chloride and **g** sulfate plotted against the groundwater temperature in the GAS

Lu^{3+} in sixfold coordination and the ionic potential of the REEs increases from 2.65 (La^{3+}) to 3.19 (Lu^{3+}), which suggest, for example, that Lu^{3+} forms stronger ionic bonds in crystals than Lu^{3+} (Faure 1991). Thus, the lanthanide contraction often reflects in a systematic variation of the crystal/liquid distribution coefficients of the REEs (Faure 1991).

REE abundance patterns have been extensively utilized in rock geochemical studies where, in general, the light REEs are concentrated in the late-stage felsic differentiates of magma, whereas the heavier REEs are concentrated in the early-formed mafic products (Faure 1991). Table 3 shows the REEs analyzed in groundwaters of the GAS. One rainwater and twelve groundwater samples were chemically analyzed for the REEs abundance patterns. The following REE ranges above the detection limit were found in groundwaters (Table 3): La = 15–281 ng/L; Ce = 18–494 ng/L; Nd = 7−276 ng/L; Sm = 0.6−46 ng/L; Eu = 1−25 ng/L; Gd = 3−47 ng/L; Dy = 4−29 ng/L; Er = 2−13 ng/L; Yb = 1−7 ng/L; Lu = 0.3−1 ng/L. Figure 6 shows that, in general, the REEs abundance patterns indeed decrease with increasing atomic number from La to Lu, as often seen in the continental crust (Faure 1991). Table 4 shows a matrix of the Pearson correlation coefficients (r) for all REEs analyzed. The two-tailed P value was estimated by GraphPad software (Arsham 1988) from each Pearson correlation coefficient. Statistically significant correlations (practically 50% of the cases showing the coherence of the REE variations) are highlighted in bold in Table 4.

The REEs concentration values are found highest at the monitoring point BCS (Table 4, Fig. 6). In this area, the

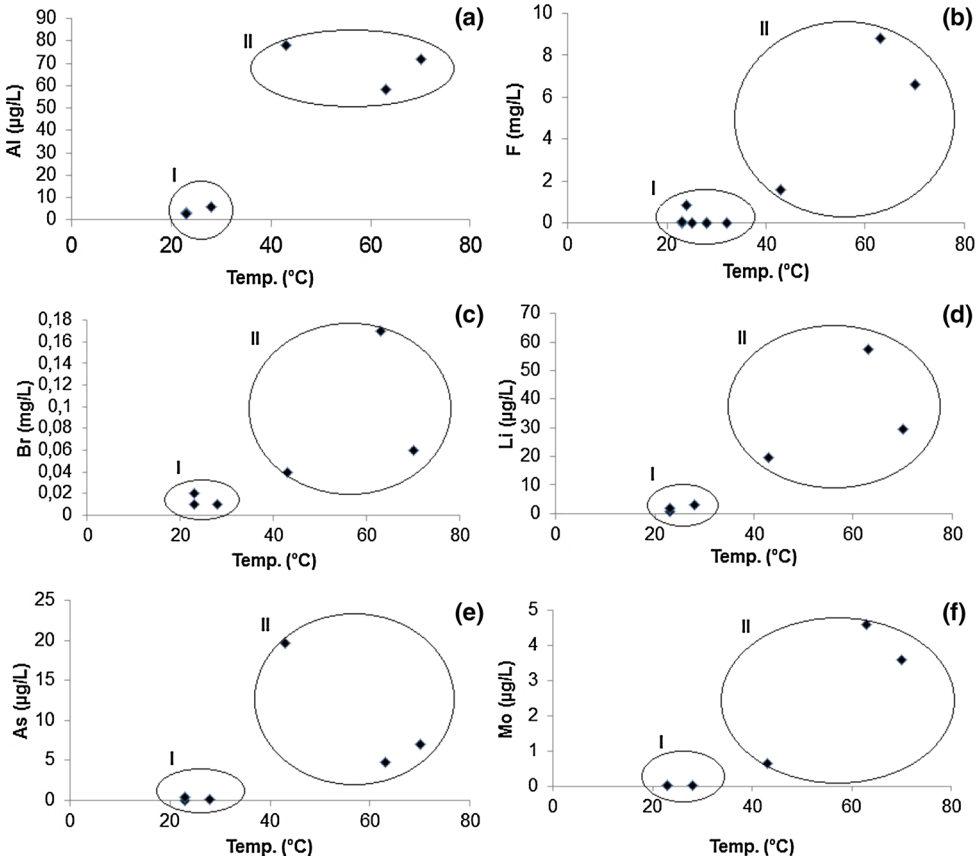

Fig. 5 Dissolved **a** aluminum, **b** fluoride, **c** bromide, **d** lithium, **e** arsenic and **f** molybdenum plotted against the groundwater temperature in the GAS

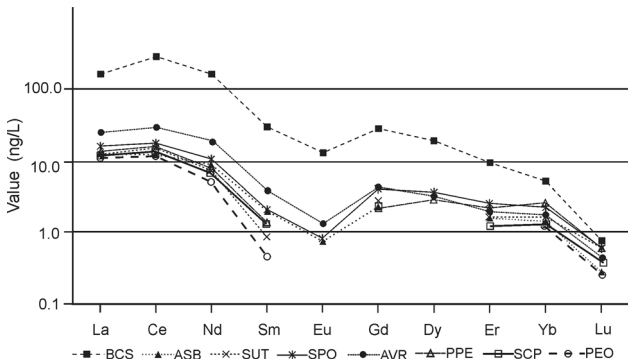

Fig. 6 REEs abundance in groundwater from the GAS. Codes: BCS, Bernardino de Campos; ASB, Águas de Santa Bárbara; SUT, Sarutaiá; SPO, São Pedro; AVR, Avaré; PPE, Presidente Prudente; SCP, Santa Cruz do Rio Pardo; PEO, Presidente Epitácio

occurrence of extensive faulting has affected the relative positioning of the layers of basalts (Serra Geral Formation) and sandstones (Botucatu and Pirambóia Formations) (Guedes et al. 2015) (Fig. 2). Such processes have exposed rock surfaces containing some minerals assembly enriched in REEs whose transfer to the liquid phase would be favored by preferential paths of leaching that could allow the REEs to be more accessible to water.

Much of the knowledge of magmatic processes and natural aqueous systems based on the relative abundance of individual lanthanide elements has been made using a logarithmic plot of lanthanide abundances normalized to abundances in chondritic (stony) meteorites (Hedrick and Templeton 1991), primordial mantle (Sun and McDonough 1989), UCC—Upper Continental Crust (Taylor and McLennan 1985), PAAS—Post Archean American Shale (Taylor and McLennan 1985), NASC—North American Shale Composite (Goldstein and Jacobsen 1988) and 3SA—3-Shale Average (Sholkovitz 1988). Recent studies focusing on the REEs distribution in groundwater have adopted the normalization to shales (Smedley 1991; Johannesson et al. 1996, 1997; Tang and Johannesson 2006).

Squisato et al. (2009) report the REEs concentration in flood basalts of Serra Geral Formation occurring in four different regions of São Paulo State (Jaú, Ribeirão Preto, Franca and Fernandópolis), which represent almost the total area of outcrops of basalts in the São Paulo State. The mean values were: La = 30.0 µg/g; Ce = 66.2 µg/g; Nd = 37.4 µg/g; Sm = 8.0 µg/g; Eu = 2.5 µg/g; Gd = 7.5 µg/g; Dy = 6.8 µg/g; Er = 3.5 µg/g; Yb = 2.8 µg/g; Lu = 0.4 µg/g. Figure 7 shows that these average values are very well correlated ($r = 0.99$) with the NASC data (Table 3), thus justifying the NASC normalization of the lanthanides abundance in groundwater. The NASC-normalized REEs abundance is also given in Table 3.

Table 4 Correlation matrix involving the REEs in GAS groundwater, São Paulo State, Brazil

La	1.00									
Ce	**0.99**	1.00								
Nd	**0.99**	**0.99**	1.00							
Sm	**0.99**	**0.99**	**0.99**	1.00						
Eu	0.41	0.44	0.41	0.47	1.00					
Gd	0.68	0.64	0.60	0.64	0.33	1.00				
Dy	**0.99**	**0.99**	**0.98**	**0.99**	**0.91**	0.66	1.00			
Er	**0.95**	**0.92**	**0.91**	**0.92**	0.41	**0.87**	**0.97**	1.00		
Yb	**0.73**	**0.68**	0.65	**0.69**	0.30	**0.94**	0.74	**0.89**	1.00	
Lu	0.36	0.34	0.29	0.34	0.67	**0.73**	0.39	0.54	0.66	1.00
	La	Ce	Nd	Sm	Eu	Gd	Dy	Er	Yb	Lu

Statistically significant correlations are highlighted in bold

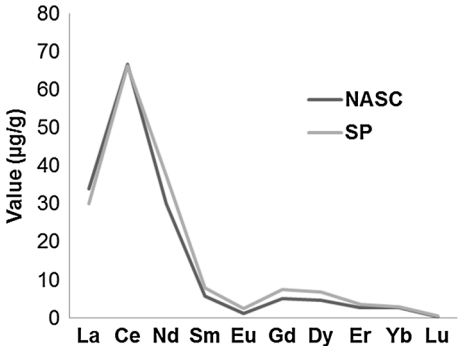

Fig. 7 Average REEs concentration in flood basalts of Serra Geral Formation occurring in São Paulo State (SP—Squisato et al. (2009) compared to the NASC, North American Shale Composite (Goldstein and Jacobsen 1988)

Eu-anomalies (Eu/Eu*) from the available data in this paper are defined as the ratio between measured Eu in the groundwater and the value expected for Eu on a smooth NASC-normalized plot. The Eu-anomalies (Eu/Eu*) have been calculated in four sites where all REEs analyzed were above the DL. This was done using the simple arithmetic $[(Sm_N + Gd_N)/2]$ mean to estimate Eu*, where Sm_N and Gd_N are the NASC-normalized values for Sm and Gd. Positive Eu-anomalies (mean Eu/Eu* = 1.6) were found: ITI = 1.8; SPO = 1.2; AVR = 1.4; BCS = 2.0 in line with SantÁnna et al. (2006) where Eu/Eu* ratio of 1.5 is shown in some highly crystalline illite-type clays occurring in sedimentary rocks of the Rio Bonito Formation (Permian), Paraná basin, which are characterized by high water/rock ratios. These findings suggest that water–rock processes taking place in the GAS strata could release REEs into the liquid phase, which retain equivalent signatures to those seen in the mineral assembly of the rock matrices.

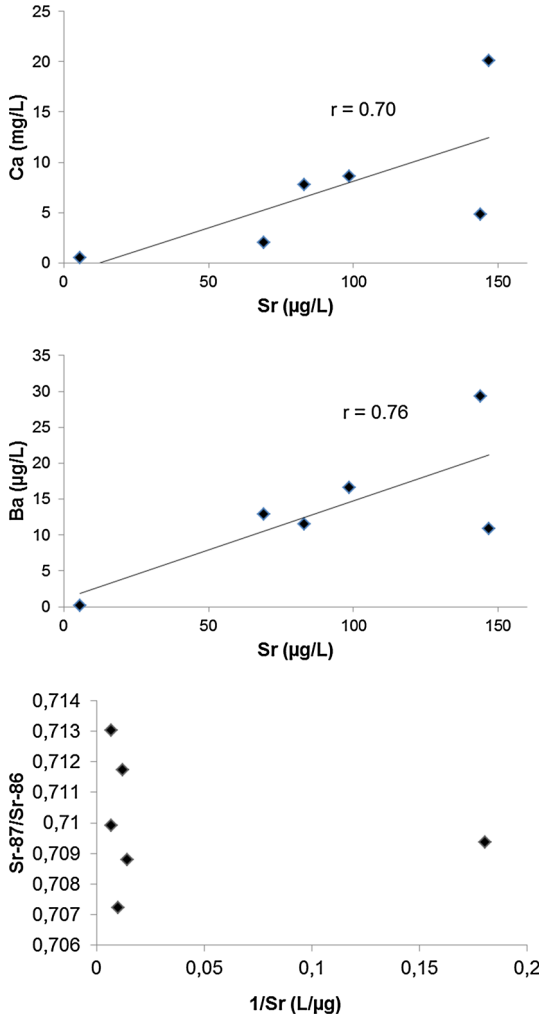

Fig. 8 Dissolved (*top*) calcium and (*middle*) barium content plotted against the strontium concentration in GAS groundwater. The $^{87}Sr/^{86}Sr$ ratio is also plotted in the *bottom* against the reciprocal of the dissolved strontium content

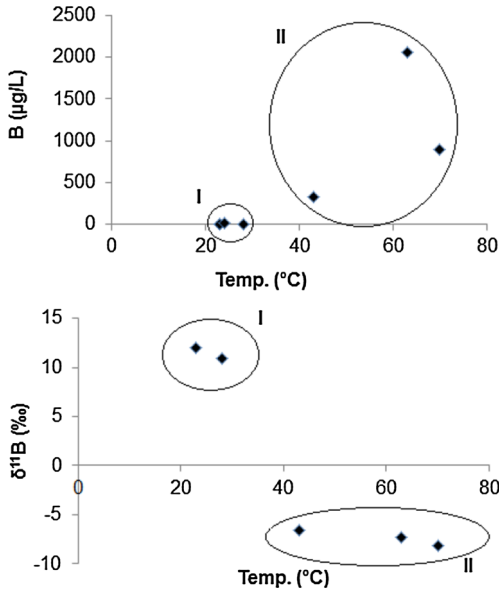

Fig. 9 (*top*) Dissolved boron and (*bottom*) $\delta^{11}B$ plotted against the groundwater temperature in the GAS

Strontium and boron isotopes in groundwater

Dissolved strontium in the groundwater behaves like other alkaline earth metals such as calcium and barium as evidenced by the significant regression correlations between them (Fig. 8). There is a decrease in both Sr and Ba contents in PPA hyperthermal waters, possibly following the same trend for higher dissolved Ca in cold/hypothermal waters SUT, SCP, ASB and BCS (Table 2). This could be attributed to the decrease in the carbonates reactivity in aqueous solution, according to increased temperature (Pokrovsky et al. 2009). The hyperthermal waters tend to exhibit restricted range $^{87}Sr/^{86}Sr$ ratios (between 0.7088 and 0.7099) (Table 2, Fig. 8) similar to the value of ca. 0.709 for seawater Sr isotopic ratio at the end of Proterozoic (between 610 and 550 Ma; Asmerom et al. 1991) although there is no evidence of a seawater component from other chemistries.

The $^{87}Sr/^{86}Sr$ ratios in the cold/hypothermal waters, however, differ from the values found in the hyperthermal waters (Table 2, Fig. 8). The carbonates reactivity increases in the lower temperatures, and leaching processes are expected to be more pronounced. The ratio in AVR cold groundwater (0.7072) approaches the mean value of 0.7065 ± 0.0006 reported by Wildner et al. (2006) for 18 samples of basaltic lavas belonging to the Serra Geral Formation and sampled at southwestern of Paraná State. On the other hand, the higher $^{87}Sr/^{86}Sr$ ratios (0.7117 and 0.7130) in the cold (SUT) and hypothermal (BCS) waters correspond to more enriched ^{87}Sr radiogenic values possibly generated from leaching of secondary calcite phase in the Botucatu/Pirambóia sandstones. This is supported by the $^{87}Sr/^{86}Sr$ ratios (0.7161–0.7171) given by Vieira (1980) and Gilg et al. (2003) in sandstones of these formations. Additionally, in studies made in the Great Artesian Basin (Australia) this was also found as de Caritat et al. (2005) suggested that $^{87}Sr/^{86}Sr$ ratios from 0.712 to 0.715 indicate the influence of carbonate dissolution, which partly includes our samples. However, Moya et al. (2016) lowered the 0.712 limit from de Caritat et al. (2005), correlating with all our "more radiogenic samples."

Boron stable isotopes (atomic masses of 10 and 11) possess natural abundances of about 19.82 and 80.18%, respectively (Mather and Porteous 2001). Boron isotope fractionations are often controlled by the partitioning between the undissociated boric acid, $B(OH)_3$ (planar trigonal) and the anion $B(OH)_4^-$ (tetrahedral), through the equilibrium reaction: $B(OH)_3 + OH^- = B(OH)_4^-$ (Pennisi et al. 2006a). Both dissolved species are pH dependent and, at 25 °C and B concentration of 10^{-3} mol.L^{-1}, $B(OH)_3$ is dominant for $pH < 9$, whereas $B(OH)_4^-$ predominates for $pH > 9$ (Tonarini et al. 2004). In general, the combination of the isotopic fractionation in reaction involving $B(OH)_3$ and $B(OH)_4^-$ and removal of $H_4BO_4^-$ by the preferential adsorption on clay minerals (Palmer et al. 1987) constitutes the main mechanism for the large isotopic variations of B seen in natural waters (Pennisi et al. 2006a, b). In continental waters, the upper limit of the $^{11}B/^{10}B$ ratios is +59‰, as observed in Australian crater lakes (Vengosh et al. 1991), and the lower limit is −27‰, as shown in groundwater (Pennisi et al. 2006a).

Dissolved boron and $\delta^{11}B$ in the groundwater samples are plotted in Fig. 9 against temperature. Cold/hypothermal waters (Group I) show lower B contents than hyperthermal waters (Group II), following trends for the trace constituents Al, Li, F, Br, As and Mo which are enhanced in the Group II waters relative to the Group I waters (Fig. 5). The $\delta^{11}B$ ranged from −8.1 to +12.0‰, where the $\delta^{11}B$-values in the cold/hypothermal waters (Group I) are positive, in a clear distinction of the negative $\delta^{11}B$-values found in the hyperthermal waters (Group II).

Because there is no evidence of anthropogenic inputs in these groundwater samples (Hirata et al. 2011), geogenic factors are considered responsible for the large variability in the $\delta^{11}B$-values. Boron is a trace element that has been considered a good indicator of paleosalinity in sedimentation sites since the pioneering studies focusing its presence in illite (Frederickson and Reynolds 1960). High B has been already identified in deep waters and Paleozoic sediments of the Paraná sedimentary basin (Ramos and Formoso 1975; Rodrigues and Quadros 1976; Szikszay and Teissedre 1981). In the current transect, the boron content increases from Rio Bonito Formation up to the Irati Formation (Rodrigues and Quadros 1976) and illite is the dominant clay mineral in sediments of the Passa Dois,

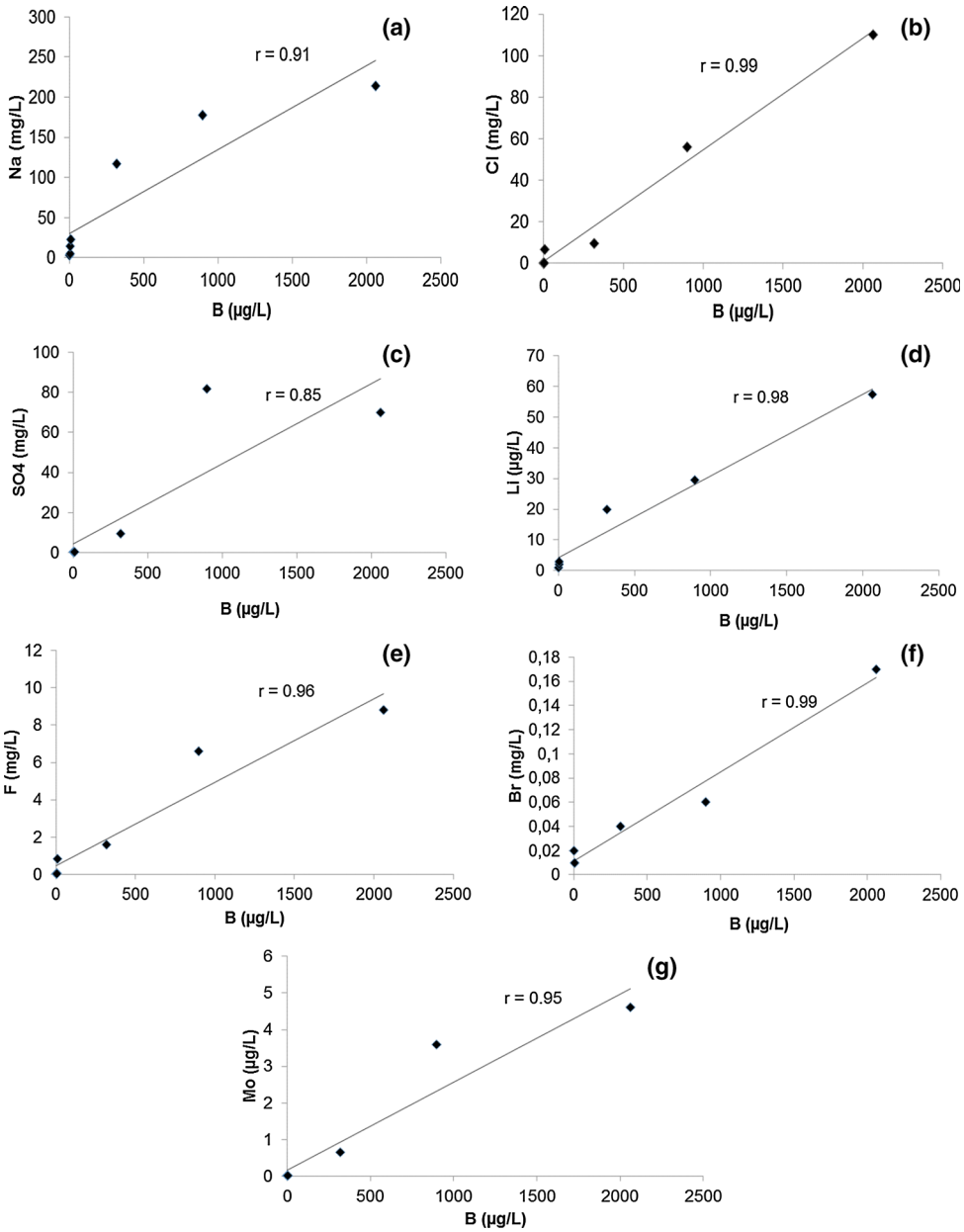

Fig. 10 Dissolved **a** sodium, **b** chloride, **c** sulfate, **d** lithium, **e** fluoride, **f** bromide and **g** molybdenum plotted against the boron content in GAS groundwater

Tubarão and Paraná Groups in bore PPA (cf. Ramos and Formoso 1975).

Boric acid, $B(OH)_3$, undergoes adsorption–desorption processes on the ubiquitous clay minerals (Pennisi et al. 2006b). ^{11}B separates preferentially into the $B(OH)_3$ species in solution, prevailing at lower pHs (Spivack and Edmond 1987; Palmer et al. 1987; Tonarini et al. 2004). This could explain the positive $\delta^{11}B$-values found in the cold/hypothermal waters (Table 2; Fig. 9).

Adsorption depends on higher pHs, prevailing $B(OH)_4^-$ that is more easily adsorbed than its equilibrium competitor $B(OH)_3$ (Pennisi et al. 2006b). ^{10}B is dominantly incorporated into $B(OH)_4^-$ in the solid phase, which substitutes for Al in silicate minerals (Spivack and Edmond 1987; Palmer et al. 1987). Water desorption from clays is a function of burial depth (geostatic/lithostatic pressure) in sediments, i.e., the number of adsorbed water layers decreases as the temperature and pressure of the sediments increase (Velde 1992). Thus, desorption processes affecting clay minerals and occurring at higher temperatures could support the negative $\delta^{11}B$-values found in the hyperthermal waters (Table 2; Fig. 9). Such processes would also explain the enhanced concentrations of some major/trace constituents in the hyperthermal waters (Group II) relative to the cold/hypothermal ones (Group I) (Figs. 4, 5) as confirmed by significant regression correlations with

boron (Fig. 10): Na ($r = 0.91$), Cl^- (0.99), SO_4^{2-} ($r = 0.85$), Li ($r = 0.98$), F ($r = 0.96$), Br ($r = 0.99$) and Mo ($r = 0.95$).

Conclusions

Groundwaters of the Guarani Aquifer System (GAS) are an important resource in South America and are extensively used for drinking water. This investigation was realized in a single transect in São Paulo State, Brazil, and involved the sampling of several boreholes drilled for exploiting the GAS. Two major water groups were identified according to temperature: cold/hypothermal waters (Group I) and hyperthermal waters (Group II). The Group I waters show geostatic pressure <100 bar, dissolved O_2 >6 mg/L, positive Eh values, EC <160 µS/cm, sodium <23 mg/L, chloride <7 mg/L and sulfate <0.5 mg/L. The trace constituents Al, Li, F, Br, As and Mo are enhanced in the Group II waters relative to the Group I waters. When comparing the hydrochemical data in groundwater to WHO guideline values for chemicals that are of health significance in drinking water (nitrate, fluoride, boron, barium, chromium, arsenic, uranium ^{226}Ra and ^{222}Rn), it was possible to identify concentrations exceeding the maximum allowable fluoride in some hyperthermal waters, as well for arsenic in one groundwater sample (PPA). However, none of these waters is used for human consumption, only for recreation (thermal swimming pools) purposes. The REEs concentration values are higher at the monitoring point BCS characterized by extensive faulting that has affected the relative positioning of the layers of basalts/sandstones from the Serra Geral Formation and Botucatu–Pirambóia Formations. Positive Eu-anomalies were found at ITI, SPO, AVR and BCS that are compatible with values reported in some highly crystalline illite-type clays occurring in sedimentary rocks of the Rio Bonito Formation (Permian), Paraná basin characterized by high water/rock ratios. $^{87}Sr/^{86}Sr$ ratios in the cold/hypothermal waters are different of the values found in the hyperthermal waters. Desorption processes affecting clay minerals at higher temperatures as shown along the studied transect could explain the negative $\delta^{11}B$-values found in the hyperthermal waters. Such processes also would explain the enhanced concentrations of some major/trace constituents in the hyperthermal waters relative to the cold/hypothermal ones.

Acknowledgements FAPESP (Foundation Supporting Research in São Paulo State) and CNPq (National Council for Scientific and Technologic Development) in Brazil are greatly thanked for financial support of this investigation. Reinhard Jung from Hochschule Mannheim, Germany, is thanked by the REE analysis made at LABOGEO/IGCE-UNESP-Rio Claro. Avner Vengosh from Duke University, USA, is thanked by ICP-MS and TIMS analyses. One anonymous reviewer is greatly thanked by helpful comments that improved the readability of the manuscript.

References

Almeida FFM, Melo MS (1981) The Paraná basin and Mesozoic volcanism. In: IPT (Technological Research Institute of São Paulo State) (ed) Geological map of São Paulo State, vol 1. Promocet, São Paulo, pp 46–81

Arsham H (1988) Kuiper's P-value as a measuring tool and decision procedure for the goodness-of-fit test. J Appl Stat 15(3):131–135

Asmerom Y, Jacobsen SB, Knoll AH, Butterfield NJ, Swet K (1991) Strontium isotopic variations of Neoproterozoic seawater: implications for crustal evolution. Geochim Cosmochim Acta 55:2883–2894

Baas Becking LGM, Kaplan IR, Moore D (1960) Limits of the natural environment in terms of pH and oxidation-reduction potential. J Geol 68:243–284

Bonotto DM (2004) Doses from ^{222}Rn, ^{226}Ra, and ^{228}Ra in groundwater from Guarani aquifer, South America. J Environ Radioact 76:319–335

Bonotto DM (2006) Hydro(radio)chemical relationships in the giant Guarani aquifer, Brazil. J Hydrol 323:353–386

Bonotto DM (2011) Natural radionuclides in major aquifer systems of the Paraná sedimentary basin, Brazil. Appl Radiat Isot 69:1572–1584

Bonotto DM (2012) A comparative study of aquifer systems occurring at the Paraná sedimentary basin, Brazil: major hydrochemical trends. Environ Earth Sci 67:2285–2300

Bonotto DM (2013) A comparative study of aquifer systems occurring at the Paraná sedimentary basin, Brazil: U-isotopes contribution. Environ Earth Sci 68:1405–1418

Bonotto DM, Armada PCP (2008) Radon and progeny (^{214}Pb and ^{214}Bi) in urban water-supply systems at São Paulo State, Brazil. Appl Geochem 23:2829–2844

Bonotto DM, Bueno TO (2008) The natural radioactivity in Guarani aquifer groundwater, Brazil. Appl Radiat Isot 66:1507–1522

Bonotto DM, Caprioglio L (2002) Radon in groundwaters from Guarany aquifer, South America: environmental and exploration implications. Appl Radiat Isot 57:931–940

Bonotto DM, Mello CB (2006) A combined method for evaluating radon and progeny in waters and its use at Guarani aquifer, São Paulo State, Brazil. J Environ Radioact 86:337–353

Bonotto DM, Bueno TO, Tessari BW, Silva A (2009a) The natural radioactivity in water by gross alpha and beta measurements. Radiat Meas 44:92–101

Bonotto DM, Caprioglio L, Bueno TO, Lazarindo JR (2009b) Dissolved ^{210}Po and ^{210}Pb in Guarani aquifer groundwater, Brazil. Radiat Meas 44:311–324

Castany G (1982) Principles and methods in hydrogeology. Dunod, Paris

Chatam JR, Wanty RB, Langmuir D (1981) Groundwater prospecting for sandstone-type uranium deposits: the merits of mineral-solution equilibria versus single element tracer methods. US DOE, Rep. GJBX-129 (81), p 216

Cowart JB, Osmond JK (1980) Uranium isotopes in groundwater: their use in prospecting for sandstone-type uranium deposits. US DOE, Rep. GJBX-119 (80), p 112

Cresswell RG, Bonotto DM (2008) Some possible evolutionary scenarios suggested by Cl-36 measurements in Guarani aquifer groundwaters. Appl Radiat Isot 66:1160–1174

de Caritat P, Kirste D, Carr G, McCulloch M (2005) Groundwater in the Broken Hill region, Australia: recognising interaction with

bedrock and mineralisation using S, Sr and Pb isotopes. Appl Geochem 20:767–787

DFPM (Division for Supporting the Mineral Production) (1966) The mining code, the mineral waters code and how applying research in a mineral deposit, 8th edn, Rep. 91, Rio de Janeiro, DFPM, p 109

Faure G (1991) Principles and applications of inorganic geochemistry. MacMillan Publishing Co, New York, p 626

Foster S, Kemper K, Garduño H, Hirata R, Nanni M (2006) The Guarani aquifer initiative for transboundary groundwater management. Case profile collection, 9, sustainable groundwater management—lessons from practice. The World Bank, Washington, DC

Frederickson AF, Reynolds RC (1960) Geochemical method of determining paleosalinity. Clay Miner 8:203–213

Gastmans D, Chang HK, Hutcheon I (2010a) Stable isotopes (^{2}H, ^{18}O and ^{13}C) in groundwaters from the northwestern portion of the Guarani Aquifer System (Brazil). Hydrogeol J 18:1497–1513

Gastmans D, Chang HK, Hutcheon I (2010b) Groundwater geochemical evolution in the northern portion of the Guarani Aquifer System (Brazil) and its relationship to diagenetic features. Appl Geochem 25:16–33

Gilg HA, Morteani G, Kostitsyn Y, Preinfalk C, Gatter I, Strieder AJ (2003) Genesis of amethyst geodes in basaltic rocks of the Serra Geral Formation (Ametista do Sul, Rio Grande do Sul, Brazil): a fluid inclusion, REE, oxygen, carbon, and Sr isotope study on basalt, quartz, and calcite. Miner Deposita 38:1009–1025

Goldstein SJ, Jacobsen SB (1988) Rare earth elements in river waters. Earth Planet Sci Lett 89:35–47

Guedes C, Morales N, Etchebehere MLC, Saad AR (2015) Indications of neotectonic deformations at Rio Pardo-SP basin by the analysis of fluvial morphometric parameters and SRTM images. Geociências 34(3):364–380

Hedrick JB, Templeton DA (1991) Rare earth minerals and metals in 1989. USBM, Washington, DC

Hirata R, Gesicki A, Sracek O, Bertolo R, Giannini PC, Aravena R (2011) Relation between sedimentary framework and hydrogeology in the Guarani Aquifer System in São Paulo state, Brazil. J S Am Earth Sci 31:444–456

i Gil AS, Bonotto DM (2015) Hydrochemical and stable isotopes (H, O, S) signatures in deep groundwaters of Paraná basin, Brazil. Environ Earth Sci 73:95–113

IAEA (International Atomic Energy Agency) (1996) International basic safety standards for protection against ionizing radiation and for the safety of radiation sources. Safety series, vol 15. IAEA, Vienna, p 353

Johannesson KH, Stetzenbach KJ, Hodge VF, Lyons WB (1996) Rare earth element complexation behavior in circumneutral pH groundwaters: assessing the role of carbonate and phosphate ions. Earth Planet Sci Lett 139:305–319

Johannesson KH, Stetzenbach KJ, Hodge VF (1997) Rare earth elements as geochemical tracers of regional groundwater mixing. Geochim Cosmochim Acta 61(17):3605–3618

Kendall GM, Fell TP, Phipps AW (1988) A model to evaluate doses from radon in drinking water. Radiological Protection Bulletin 97:7–8

Krauskopf KB, Bird DK (1995) Introduction to geochemistry. McGraw-Hill Inc, New York

Marques LS, Duprè B, Piccirillo EM (1999) Mantle source compositions of the Paraná Magmatic Province (southern Brazil): evidence from trace element and Sr-Nd-Pb isotope geochemistry. J Geodyn 28:439–458

Mather JD, Porteous NC (2001) The geochemistry of boron and its isotopes in groundwaters from marine and non-marine sandstone aquifers. Appl Geochem 16:821–834

Moya CE, Raiber M, Taulis M, Cox ME (2016) Using environmental isotopes and dissolved methane concentrations to constrain hydrochemical processes and inter-aquifer mixing in the Galilee and Eromanga Basins, Great Artesian Basin, Australia. J Hydrol 539:304–318

Oliveira J, Mazzilli BP, Sampa MHO, Bambalas E (2001) Natural radionuclides in drinking water supplies of São Paulo State Brazil and consequent population doses. J Environ Radioact 53:99–109

Osmond JK, Cowart JB (1981) Uranium-series disequilibrium in groundwater and core composite samples from the San Juan Basin and Copper Mountain research sites. US DOE, Rep. GJBX-364 (81), p 126

Palmer MR, Spivack AJ, Edmond JM (1987) Temperature and pH controls over isotopic fractionation during adsorption of boron on marine clays. Geochim Cosmochim Acta 51:2319–2323

Pelicho AF, Martins LD, Nomi SN, Solci MC (2006) Integrated and sequential bulk and wet-only samplings of atmospheric precipitation in Londrina, South Brazil (1998-2002). Atmos Environ 40:6827–6835

Pennisi M, Gonfiantini R, Grassi S, Squarci P (2006a) The utilization of boron and strontium isotopes for the assessment of boron contamination of the Cecina River alluvial aquifer (central-western Tuscany, Italy). Appl Geochem 21:643–655

Pennisi M, Bianchini G, Muti A, Kloppmann W, Gonfiantini R (2006b) Behaviour of boron and strontium isotopes in groundwater–aquifer interactions in the Cornia Plain (Tuscany, Italy). Appl Geochem 21:1169–1183

Pokrovsky OS, Golubev SV, Schott J, Castillo A (2009) Calcite, dolomite and magnesite dissolution kinetics in aqueous solutions at acid to circumneutral pH, 25 to 150°C and 1 to 55 atm pCO2: new constraints on CO2 sequestration in sedimentary basins. Chem Geol 265(1–2):20–32

Ramos AN, Formoso MLL (1975) Clay minerals from sedimentary rocks of the Paraná basin. PETROBRÁS-CENPES-DINTEP, Rio de Janeiro, p 72

Rodrigues R, Quadros LP (1976) Mineralogy of clays and boron content of Paleozoic formations from Paraná basin. In: SBG (Brazilian Society of Geology) (ed) Proceedings of XXIX Brazilian geological congress, vol 1. SBG, Ouro Preto, pp 351–379

SanťAnna LG, Clauer N, Cordani UG, Riccomini C, Velázquez VF, Liewig N (2006) Origin and migration timing of hydrothermal fluids in sedimentary rocks of the Paraná basin, South America. Chem Geol 230:1–21

Sholkovitz ER (1988) Rare-earth elements in marine sediments and geochemical standards. Chem Geol 88:333–347

Silva RBG (1983) Hydrochemical and isotopic study of groundwaters from Botucatu aquifer in São Paulo State. Ph.D. Thesis, USP-São Paulo University, São Paulo

Smedley PL (1991) The geochemistry of rare earth elements in groundwater from the Carnmenellis area, southwest England. Geochim Cosmochim Acta 55:2767–2779

Spivack AJ, Edmond JM (1987) Boron isotope exchange between seawater and the oceanic crust. Geochim Cosmochim Acta 51:1033–1043

Squisato E, Nardy AJR, Machado FB, Marques LS, Rocha ERV Jr, Oliveira MAF (2009) Lithogeochemistry and petrogenetic aspects of basalts from Paraná Magmatic Province at the north-central portion of São Paulo State. Geociências 28(1):27–41

Sracek O, Hirata R (2002) Geochemical and stable isotopic evolution of the Guarani Aquifer System in the state of São Paulo, Brazil. Hydrogeol J 10:643–655

Sun SS, McDonough WF (1989) Chemical and isotopic systematics of oceanic basalts: implications for mantle composition and

processes. In: Sauders MJ (ed) Magmatism in the ocean basins, vol 42. Geological Society Special Publ, London, pp 313–345

Szikszay M, Teissedre JM (1981) Springs of the Paraná sedimentary basin, São Paulo State. Revista Águas Subterrâneas 3:85–102

Tang J, Johannesson KH (2006) Controls on the geochemistry of rare earth elements along a groundwater flow path in the Carrizo Sand aquifer, Texas, USA. Chem Geol 225:156–171

Taylor SR, McLennan SM (1985) The continental crust: its composition and evolution. Blackwell, Melbourne, p 312

Tonarini S, Pennisi M, Gonfiantini R (2004) Boron isotope determinations in waters and other geological materials: analytical techniques and inter-calibration of measurements. In: IAEA (International Atomic Energy Agency) (ed) Book of extended synopses of the international symposium on quality assurance for analytical methods in isotope hydrology, Vienna, IAEA, pp 55–56

Tweed SO, Weaver TR, Cartwright I, Schaefer B (2006) Behavior of rare earth elements in groundwater during flow and mixing in fractured rock aquifers: an example from the Dandenong Ranges, southeast Australia. Chem Geol 234:291–307

Velde B (1992) Introduction to clay minerals: chemistry, origins, uses and environmental significance. Chapman & Hall, London

Vengosh A, Chivas AR, McCulloch MT (1989) Direct determination of boron and chlorine isotopes in geological materials by negative thermal-ionization mass spectrometry. Chem Geol 79:333–343

Vengosh A, Chivas AR, McCulloch MT, Starinski A, Kolodny Y (1991) Boron isotope geochemistry of Australian salt lakes. Geochim Cosmochim Acta 55:2591–2606

Vieira PC (1980) Preliminary geochronological interpretation of the Paraná basin. Revista IG 1(2):25–32

WHO (World Health Organization) (2011) Guidelines for drinking-water quality, 4th edn. WHO Press, Geneva

Wildner W, Brito RSC, Licht OAB, Arioli EE (2006) Geology and Mineral Resources from Paraná State, scale 1:200,000. Brasília, CPRM/Mineropar, p 95